Modeling and Experimental Measurement of Power Efficiency for Power-Limited SDM Submarine Transmission Systems

Hrishikesh Srinivas, *Student Member, IEEE*, John D. Downie, *Member, IEEE*, Jason Hurley, Xiaojun Liang, James Himmelreich, Jose Krause Perin, Darli A. A. Mello, *Member, IEEE*, and Joseph M. Kahn, *Fellow, IEEE*

***Abstract*—Power efficiency of long-haul optical fiber transmission has emerged as a critical challenge to cost-effectively increasing submarine cable capacity. Building on previous experimental work and informed by physical system modeling and optimization, we report on extensive amplified transmission experiments characterizing the metric of fiber capacity per unit pump power over a range of amplifier powers and link distances relevant to power-limited spatial-division-multiplexed submarine systems. We compare experimental results with modeling incorporating optical amplifier physics as well as generalized droop, demonstrating excellent agreement over the range of powers and distances tested. We predict the performance gains achievable by further optimizing the system design and implementation within tolerances ideally achieved in deployed submarine systems, and estimate fiber pair counts and total cable capacities achievable for the link distances investigated. Our results suggest the utility of amplifier pump powers as low as 20 mW and output powers as low as 6.5 dBm in reaching Pb/s cable capacities.**

***Index Terms*—Optical fiber communication, power efficiency, space division multiplexing, submarine cable capacity.**

I. Introduction

In order to meet increasing demands for trans-oceanic submarine system capacity, there have been significant recent efforts to deploy more cables with higher capacities [1]. Given the fixed-power-supply nature of submarine cables, significant attention has been focused on maximizing the power efficiency of information transmission [2]–[5]. This has led to arguments that cable capacity is increased for a given power supply limit by reducing optical amplifier output powers and thus channel signal-to-noise ratios (SNRs) at the receiver, while increasing the fiber pair count in the cable [6]–[13]. This spatial-division-multiplexing (SDM) approach follows from Shannon's capacity formula, in which capacity scales logarithmically with SNR but linearly with the number of spatial paths (or parallel fibers) over which signal power is divided. SDM has been successfully applied in long-haul transmission experiments over the past few years [3]–[5], [14]–[16]. Sinkin *et al.* in [4], [5] demonstrated the existence of a pump power maximizing power efficiency governed by a signal droop effect in constant-output-power amplifier systems, and presented the first experimental measurements of power efficiency for an exemplary C+L-band system. Here, signal droop accounts for the impact on SNR of amplified spontaneous emission (ASE) noise power, which grows along the link as it is added to at each node, contributing to amplifier saturation. Modeling of the generalized droop effect, first introduced by Antona *et al.* in [17], has extended this understanding to capture per-span noise accumulation in low-SNR systems and to accommodate different noise sources under various amplification conditions relevant to long-haul links [18], [19]. These models rely on black-box modeling of the amplifiers, abstracting away details of amplifier saturation and wavelength-dependence of gain and noise. Perin *et al.* in [20], considering fundamental Erbium-doped fiber amplifier (EDFA) physics and optimizing channel launch power spectra under the power-feed constraint, affirmed that capacity is maximized by reducing amplifier powers, and clarified the trade-off between maximizing overall capacity and optical-to-optical power conversion efficiency (PCE).

In this paper, we report on the first experiments using the system optimization approach of [20] as the basis for design and modeling of long-haul links. We follow on the earlier work with extensive transmission measurements alongside accurate physical modeling to evaluate power efficiency expressed in terms of fiber capacity per unit power consumption. The optical channels carry 48 Gbaud polarization multiplexed 16-ary quadrature amplitude modulation (PM-16QAM) or quadrature phase shift keying (PM-QPSK) signals, and we assess capacity by the bit-wise metric of generalized mutual information (GMI) [21]. The remainder of this paper is organized as follows. We describe the optimization-based design of the experimental system in Section II. In Section III, we present measured capacity and

Manuscript received October 12, 2020; revised December 4, 2020; accepted December 28, 2020. Date of publication January 6, 2021; date of current version April 16, 2021. This work was supported by Corning, Inc. The work of Darli A. A. Mello was supported by FAPESP under Grants 2018/14026-5, 2015/24341-7, and 2015/24517-8. *(Corresponding author: Hrishikesh Srinivas.)*

Hrishikesh Srinivas, Jose Krause Perin, and Joseph M. Kahn are with the E. L. Ginzton Laboratory, Department of Electrical Engineering, Stanford University, Stanford, CA 94305 USA (e-mail: hrishsri@stanford.edu; jkperin@stanford.edu; jmk@ee.stanford.edu).

John D. Downie, Jason Hurley, Xiaojun Liang, and James Himmelreich are with the Corning Research and Development Corporation, Corning, NY 14831 USA (e-mail: downiejd@corning.com; hurleyje@corning.com; liangx3@corning.com; himmelreje@corning.com).

Darli A. A. Mello is with the School of Electrical and Computer Engineering, University of Campinas (UNICAMP), Campinas 13083-852, Brazil (e-mail: darli@decom.fee.unicamp.br).

Color versions of one or more figures in this article are available at https://doi.org/10.1109/JLT.2021.3049709.

Digital Object Identifier 10.1109/JLT.2021.3049709

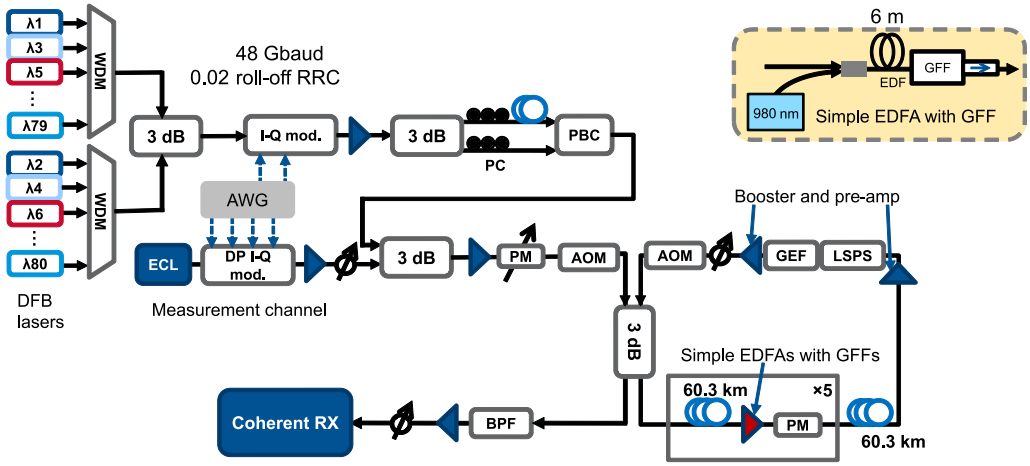

Fig. 1. Schematic diagram of the experimental system. AWG: arbitrary waveform generator, ECL: external cavity laser, PBC: polarization beam combiner, AOM: acousto-optic modulator, PM: power monitor, BPF: band-pass filter, LSPS: loop-synchronous polarization scrambler, GEF: gain equalization filter, GFF: gain-flattening filter. A schematic of the custom EDFA pumped by a 980 nm diode with designed GFF and following isolator is shown in the top right corner.

power efficiency data over a wide range of transmission distances and powers relevant to submarine systems. We demonstrate excellent agreement with simulations that combine generalized signal droop with detailed amplifier physics [20]. Finally, in Section IV we discuss limitations of the experimental system compared to realistic submarine system requirements and discuss avenues for further optimizing the experimental system. We predict the resulting system power efficiencies, estimate the numbers of parallel fiber pairs supported by SDM power-constrained cable design, and estimate the resulting total cable capacities. While some of our capacity and power efficiency measurements were presented in a short conference paper [22], the present paper provides far more measured data and explanation of optimization-based system design, physical system modeling, and consequences of our findings for power-constrained cable design than [22].

II. Experiments

We examined the potential of SDM in transmission systems optimized for capacity via experiments exploring pump powers from 14 mW to 100 mW, and link distances up to 18000 km, with a recirculating loop setup of six amplified fiber spans including custom EDFAs and closely matched gain-flattening filters (GFFs). In this section, we describe the design methodology and details of the experimental system.

A. Design Methodology

Design of the recirculating loop configuration, shown schematically in Fig. 1, was based on initial modeling and optimization derived from the insights of [20]. This approach optimizes the EDF length and signal channel input powers in order to maximize information capacity, assuming an idealized system in which all amplifiers are identical with gain and loss perfectly balanced in each span. The EDF length and signal input powers were optimized for a fixed span length of 60 km and for intermediate pump powers between 40 mW and 60 mW, although experiments were conducted for pump powers from 14 mW to 100 mW. Resource limitations in evaluating long-haul links over a wide range of powers and distances necessitated choosing a single span length for all experiments. The span length of 60 km was chosen as being suitable for the ultra-low-loss fiber used up to the longest distances studied, where feed-power limitations become prominent.

TABLE I
Erbium-Doped Fiber (EDF) Parameters

Parameter	Symbol	Value	Units
Numerical Aperture	NA	0.28	
Core radius	a	0.89	μm
Erbium doping radius	a_0	0.73	μm
Er^{3+} ion density	ρ	9.96×10^{18}	cm^{-3}
Al_2O_3 co-doping fraction		6.6	% wt.
Metastable level lifetime	τ	10	ms
Saturation parameter	ξ	3.5×10^{15}	$m^{-1}s^{-1}$
Average excess loss	l_{ex}	0.374	dB/m
980 nm pump absorption coefficient	α_p	5.336	dB/m
1529.0 nm signal absorption coefficient	α_s	7.778	dB/m
1530.5 nm signal gain coefficient	g_s^*	7.168	dB/m

Simulation of power propagation incorporated amplifier physics in each span via numerical solution of the coupled rate and propagation equations of the three-level atomic system for signal, pump, ASE (forward-propagating only assumed) and nonlinear noise powers, using the approach of Desurvire *et al.* [23]–[25]. Specific model parameters of the high-NA Erbium-doped fiber (EDF) fabricated by Corning are given in Table I, including peak values of the EDF absorption and gain coefficient spectra used to model the amplifier gain and noise. A link of up to 270 spans of fiber was simulated, providing a prediction of the gain and ASE noise evolution over all channels in the longest links. We employed a discrete form of the Gaussian Noise (GN) model [20] to approximate the accumulation of signal-related nonlinear noise in all link performance simulations. Nonlinear noise had negligible impact on the optimized system designs, confirming operation in the linear power regime.

The signal power allocation and EDF length were optimized using the particle swarm optimization (PSO) technique

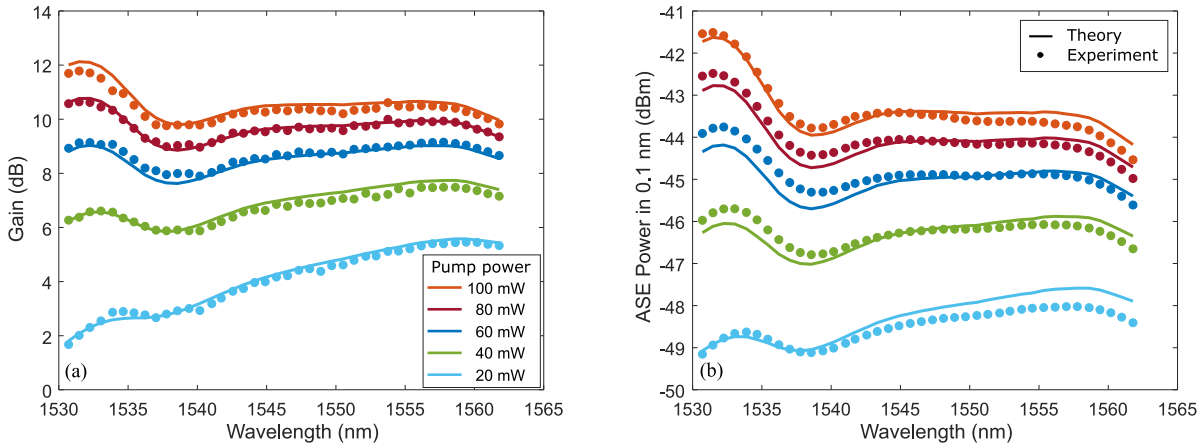

Fig. 2. Exemplar EDFA experimental and theoretical a) gain and b) ASE power in 0.1 nm, for pump powers ranging from 20 mW to 100 mW and equal input channel power −10.5 dBm in 40 channels. Theory curves were computed using the numerical three-level EDFA model [24], [25] for EDF parameters as shown in Table I, with nominal absorption and gain coefficients α and g^* scaled down by 5% (the scaling correction as described in Sections II and IV).

introduced in [20], yielding a full C-band channel plan and the chosen EDF length of about 6 m. While the optimized channel powers may be unequal in general, employing the flat mean power level across all channels was observed to cause negligible impact (less than 1%) on overall capacity. The optimization procedure assumes that all the EDFAs along the link are identical and are pumped identically, and that each EDFA is followed by a GFF that compensates its non-flat gain spectrum to ideally compensate the span loss, which is close to 10 dB. As ASE power accumulates along the link, saturating the amplifiers, the required GFF attenuation decreases by about 0.5 dB. The GFF profile at the final span of the system with 40 mW pump power was used to specify the design for manufacture of thin-film filters by AC Photonics, Inc. The GFF peak-to-peak error was less than 0.5 dB and insertion loss 0.6 dB. Gain excursion over wavelength of an EDFA+GFF unit was measured to be up to 2 dB for pump powers above 40 mW. For lower pump powers ($\leq$ 20 mW), we observed gain tilt up to about 4 dB. In Fig. 2 we present the experimental characterization data of gain and ASE power for one of the custom EDFAs in good agreement with theoretical modeling. For each of the five custom amplifiers, the nominal model values of absorption and gain coefficients α and g^* had to be scaled up or down from the measured values of the EDF, by an average of 1% and by 10.6% in the worst case, to ensure a close fit to the independently measured spectra. These amplifier coefficient scaling corrections are discussed further in Section IV.

In Fig. 3 we present the measured gain for the same EDFA without and with the GFF, whose design profile is shown in the middle panel. The spectrum is observed to be relatively flat over the nominal 40 mW to 60 mW design range of pump powers, with the largest tilt occurring at the lowest pump powers outside that range. This non-ideal gain tilt especially impacting low pump powers could be partially mitigated in our experiments by the relatively frequent use of dynamic gain equalization, and in a deployed system would be made negligible by designing the GFF profile specifically for the pump power of the system.

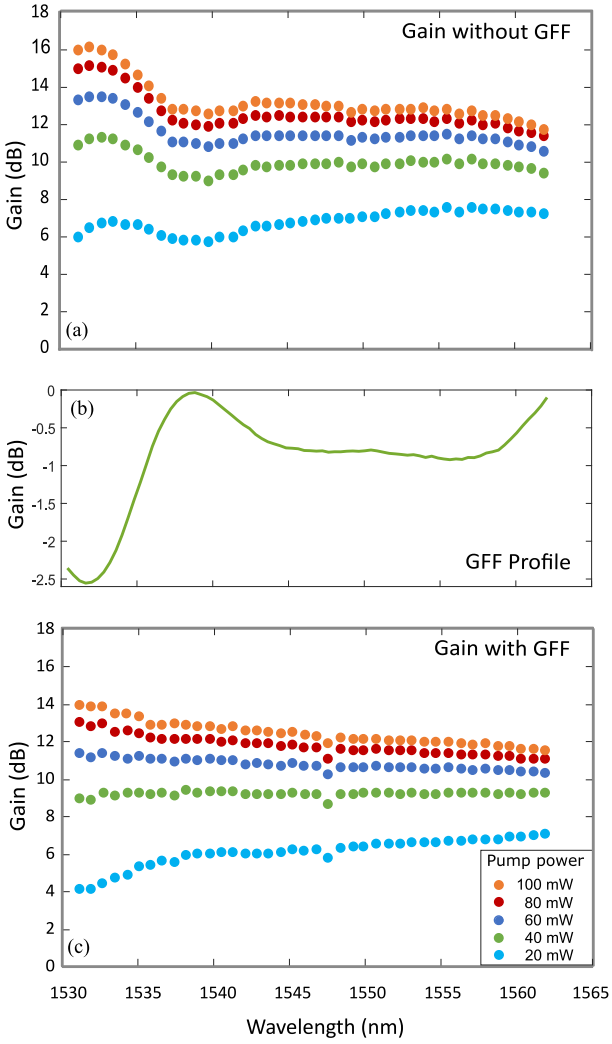

Fig. 3. Gain spectra of a) EDFA measured without GFF, b) GFF design profile, and c) EDFA measured with GFF, for pump powers ranging from 20 mW to 100 mW and equal input channel power −14.5 dBm in 40 channels. In c), the dip in gain at 1547.5 nm is an artifact of laser wavelength drift between measurements.

B. Experimental Setup

A total of 80 channels were modulated with 48 Gbaud PM-16QAM or PM-QPSK signals on a 50 GHz grid in the C-band. For most experiments, the format was 16QAM. A wavelength-tunable test channel laser with 100 kHz linewidth was modulated by one dual-polarization (DP) I-Q modulator, while the other 79 channels were modulated by another single-polarization I-Q modulator. A four-channel arbitrary waveform generator (AWG) with 42 GHz bandwidth and sampling rate of 120 GSa/s created the electrical signals that drove the I-Q modulators to create optical signals having root-raised-cosine (RRC) pulse shaping with a roll-off factor of 0.02. All four AWG channels drove the DP I-Q modulator for the test channel, while two of the negative-polarity AWG outputs created a single-polarization signal for the other 79 channels. That 79-channel set was polarization multiplexed by splitting, polarization rotating to orthogonal states, delaying one stream, and then recombining. All 80 channels were combined and amplified before launch into the recirculating loop system with a starting optical SNR (OSNR) of about 30.5 dB.

The transmission system in the loop comprised six spans of optical fiber (Corning Vascade EX3000 fiber) with an average span length of 60.3 km. The fiber effective area was 153 μm^2 and the average span loss was 9.6 dB, including connectors and splices. The first five spans in the loop were each followed by a custom EDFA built from 6 m of 0.28-NA EDF, single forward-propagating 980 nm pump laser, 980/1550 nm WDM, GFF including output isolator, and inline power monitor. These simple EDFAs were operated with pump powers set to produce a given total output power, and were measured to have an average noise figure of less than 5.5 dB for all pump powers with a tilt of about 1 dB across the band. The sixth span was followed by a commercial two-stage EDFA with loop-synchronous polarization scrambler (LSPS) and tunable gain equalization filter (GEF) included in the mid-stage. This two-stage amplifier was not adjusted for different launch conditions. We measured its effective noise figure, increasing with pump power in the simple EDFAs, from 5.5 dB at 14 mW to 8.2 dB at 100 mW. The required mid-stage GEF attenuation profile was set with pump power as shown in Fig. 4. At the output of the loop, the channel under test was selected by a band-pass filter (BPF) and directed into a coherent optical receiver. The electrical output signals were sampled by a pair of 65 GHz bandwidth oscilloscopes with a sampling rate of 160 GSa/s. The waveforms were processed offline using blind digital signal processing (DSP) algorithms, and GMI was estimated from the recovered signal constellations.

III. Results

Measurement data was collected as a function of transmission distance and EDFA output power. The output powers as indicated by the power monitors and corresponding average pump powers used are given in Table II.

Spectral efficiency (SE) in b/s/Hz can be computed for symbol rate R_s and channel spacing Δf as

$$\mathrm{SE} = \mathrm{GMI}\frac{R_s}{\Delta f}. \tag{1}$$

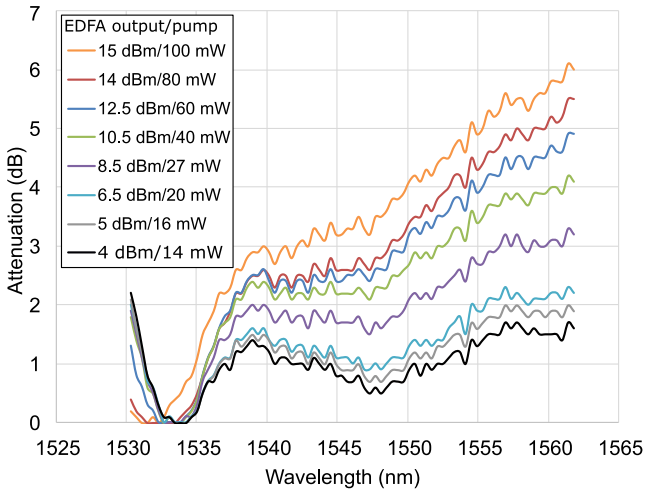

Fig. 4. Sixth span mid-stage GEF attenuation spectra in the loop set for the different pump powers in the experiment, from 14 mW to 100 mW.

TABLE II
CHANNEL, EDFA OUTPUT, AND PUMP POWERS IN EXPERIMENTS

Channel power (dBm)	EDFA output (dBm)	Pump power (mW)
−15	4	14
−14	5	16
−12.5	6.5	20
−10.5	8.5	27
−8.5	10.5	40
−6.5	12.5	60
−5	14	80
−4	15	100

The total capacity in Tb/s is given by the average SE multiplied by the 4 THz bandwidth, and can also be written in terms of the average GMI over the $N_{\mathrm{ch}} = 80$ channels, denoted by $\mathrm{GMI}_{\mathrm{av}}$, as

$$C = \mathrm{GMI}_{\mathrm{av}} \cdot R_s \cdot N_{\mathrm{ch}}. \tag{2}$$

All 80 optical channels were measured in the case of EDFA output power 10.5 dBm and 40 mW average pump power for a subset range of four transmission distances, with the results and corresponding average SE at the four distances shown in Fig. 5. The SE at 10860 km, for which the power efficiency is close to optimal (see Fig. 9. d)), exhibits a peak-to-peak variation of roughly 2 b/s/Hz over wavelength about the mean value of 3.02 b/s/Hz, corresponding to peak-to-peak OSNR variation across the band of roughly 4.8 dB. For lower pump powers ($\leq$ 20 mW), this peak-to-peak OSNR variation could be up to 6 dB larger due to imperfect gain flattening.

For each output power level, we measured the GMI of 10 equally spaced and representative channels across the full 80-channel plan, for loop numbers in multiples of five. The measured 10-channel average SE data for the four distances shown in Fig. 5 were essentially identical to the results found from the full 80-channel measurements, providing confidence in the accuracy of the technique of sampling 10 channels. For the maximum studied EDFA output power of 15 dBm, the transmission distance extended to more than 18000 km, but was

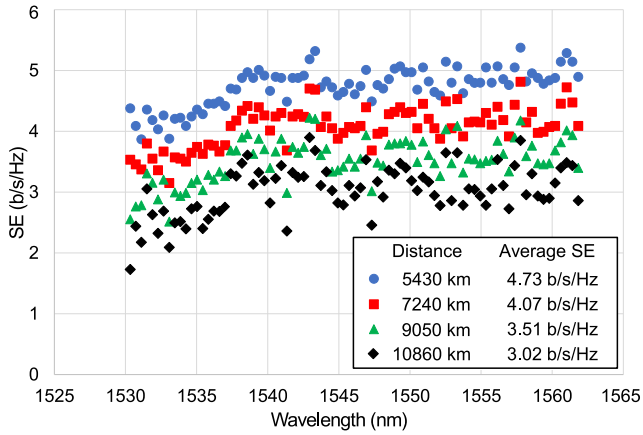

Fig. 5. Spectral efficiency (SE) in b/s/Hz of all 80 channels for 40 mW pump power, 10.5 dBm output power at 5430 km, 7240 km, 9050 km, and 10860 km link distances with corresponding average SE values shown.

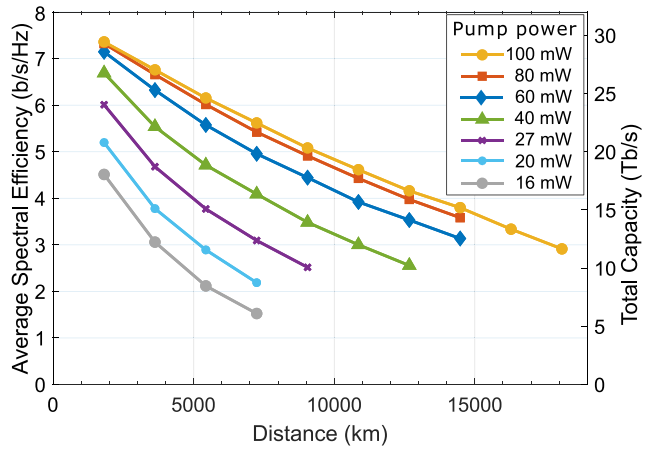

Fig. 6. Measured average SE (left ordinate) and total capacity (right ordinate) vs. link distance in the case of PM-16QAM signal format, for the different pump powers in the experiment from 16 mW to 100 mW.

shorter for lower output power levels where SNRs became too low for DSP to function effectively. The results for PM-16QAM transmission measurements are summarized in Fig. 6 in terms of average SE and total capacity with transmission distance. The GMI vs. OSNR is compared against ideal theory for both modulation formats in Fig. 7. Deviations of the experimental data from the ideal GMI theory curves in Fig. 7 represent the implementation penalties of the transmitter and receiver in a back-to-back configuration for the two modulation formats.

We calculated a metric of power efficiency (capacity per unit power consumption) for the range of output powers and link distances. The power efficiency (PE) metric is taken in this study as fiber capacity divided by pump power of a single EDFA, C/P_p in Tb/s/mW. Pump power is directly related to electrical power consumed assuming the pump lasers achieve high wall-plug efficiency independent of pump power, as might be facilitated by pump farming [26]. Results for all PM-16QAM measurements are shown in Fig. 8 down to an average pump power of 16 mW, illustrating that lower output and pump powers can yield significantly higher power efficiency, depending on link length. Lower pump powers enable higher fiber counts and overall system capacity for a given link length and fixed power supply, with the limit set by the existence of an optimum pump power and EDFA output power governed by the signal droop effect at low powers.

We also performed theoretical modeling of the experiments by numerical simulation of the power propagation in each link of a given distance and pump power, computing amplifier gain and noise using the three-level amplifier physical model [24], [25] for each of the five custom amplifiers and assuming constant-output-power black-box operation for the amplification in the sixth span (modeling the commercial dual-stage amplifier with mid-stage dynamic gain equalization). We used a generalized droop model [17]–[19] for the per-span OSNR evolution in each link, and included an additional loss of no more than 1 dB in each of the custom spans to account for the power monitor and GFF insertion losses. The EDFA excess losses were specific to each of the five custom amplifiers, with their average value shown in Table I. Our modeling further accounted for inhomogeneities between spans including the six different span lengths and span losses, as well as custom amplifier absorption and gain coefficients. The coefficient scaling corrections introduced in Section II ensured a close fit between the numerically modeled and experimentally measured gain and noise spectra for each amplifier as shown for example in Fig. 2, and revealed excellent agreement with experimental measurements of capacity C and capacity per unit pump power C/P_p over most of the experimental conditions, particularly near the optimum pump power where the effect of signal droop becomes most prominent. Fig. 8 demonstrates this close agreement between experiment and theory for the PE metric against transmission distance. Slight discrepancies emerge at the lowest pump powers and at the longest link distance, where small deviations in per-span noise contributions have a larger impact on SE.

In Fig. 9, we show the measured results at the intermediate link distances of 5430 km, 7240 km, 9050 km and 10860 km against detailed modeling simulations incorporating amplifier physics as described above. For comparison, we also performed simplified modeling assuming black-box EDFAs with constant average noise figure, i.e., including only the effect of generalized droop under constant amplifier output power operation, as developed in [18], [19]. Both detailed and simplified modeling included accurately measured implementation penalty, or gap-to-GMI, data for both signal formats, as well as optical-to-optical PCE of the EDFAs. The SNR at the end of the link was used to calculate the achievable constrained capacity of GMI and the metric of capacity per unit pump power C/P_p. We included experimental data obtained for QPSK signals at the lowest output power levels, where the models predict higher capacity and capacity per unit power for QPSK than 16QAM. At distances of 7240 km, 9050 km and 10860 km, one other QPSK data point was also taken at a higher pump power of 60 mW to test the validity of our modeling. The agreement between the measured data and simulation is excellent, and agreement with the simplified model assuming only generalized droop for uniform constant-output-power black-box amplifiers is within 10% or better for the range of powers tested. Analysis of both experimental and modeling

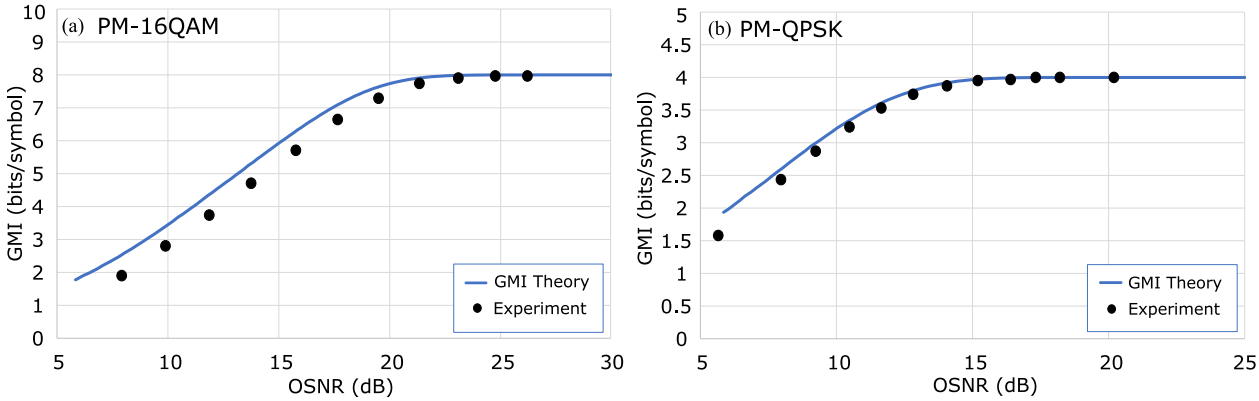

Fig. 7. Information rate in two polarizations as GMI in bits/symbol vs. OSNR in dB, for a) PM-16QAM, and b) PM-QPSK modulation formats. Ideal GMI theory is shown as the solid blue curves, while experimental Tx-Rx measurements, which are subject to format-specific implementation penalties also incorporated in modeling, are plotted as the black filled-circle data points.

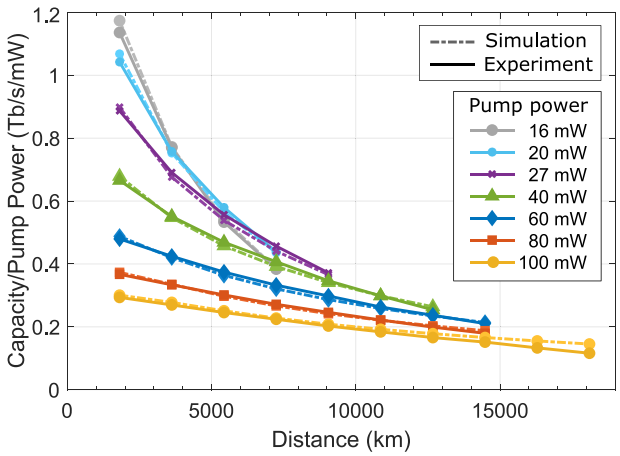

Fig. 8. Average power efficiency (PE) results in the case of PM-16QAM signal format, in terms of total capacity per unit pump power C/P_p against link distance for the different pump powers in the experiment from 16 mW to 100 mW. Solid lines connect the experimental data points, while lighter dot-dashed lines connect the theoretical modeling simulation results of the same link parameters.

results verifies that PE expressed as capacity per unit pump power is maximized at lower pump powers between 12 dBm and 14 dBm depending on link length, at the cusp between regimes of low and high optical-to-optical amplifier PCE.

IV. Discussion

In addition to being power-limited, submarine transmission systems must operate with stringent tolerance and reliability requirements in order to guarantee stable performance over their decades-long lifetimes. Some of these requirements were not well-satisfied in the experimental setup due to limitations in available equipment. In this section, we describe some of these limitations and consider the performance gains achievable under more idealized experimental conditions, in particular those of pump laser stability and tunable gain flattening.

A. Experimental Limitations

Submarine EDFAs are forward-pumped at 980 nm for high gain efficiency and low noise figure, with an isolator placed at the amplifier input in addition to the GFF output to minimize backward-propagating ASE power [27]. Our setup did not include isolators at the amplifier inputs, however the impact of backwards-ASE generated in the EDFAs was negligible in the experiments and could be neglected in modeling. Submarine systems use fiber Bragg gratings to stabilize the pump lasers, resulting in wavelength drifts of less than 0.4 nm so that pump absorption by the EDF is kept almost entirely within the pump band [28]. In our setup, error in the wavelengths of the available pump lasers resulted in greater inhomogeneity between the spans. The scaling applied to each EDFA's absorption and gain coefficients in simulations of the experiments accounted for differences in the operative coefficients induced by error or drift in the diode laser wavelengths, which was roughly ± 1.8 nm. Stabilization of the pump laser wavelengths to 980 nm within an error of ± 0.2 nm would result in a more ideal system with higher PE.

The experimental setup was also limited by the use of GFFs designed for a narrow range of pump powers. By comparing the difference between the experimental GEF profiles (Fig. 4) and wavelength-selective GEF profiles in simulation, which assumed ideal gain equalization at every sixth span, we estimated the additional gain tilt after each circulation of the loop to be no more than 5 dB in all cases. This was the largest value of gain difference corrected prior to subsequent recirculation, and could be made lower by tailoring design of the GFFs for each pump power, and by improving insertion loss and GFF error performance, which in submarine systems have peak-to-peak errors as low as 0.1 dB [29]. While GFFs have inherent loss and directly impact the EDFA output power, their use in long-haul systems allows the maximal usable bandwidth and hence number of transmitted channels, ensures that the signal power spectrum does not acquire a large tilt over successive spans, and limits the accumulation of ASE power, thereby reducing the amount of variability in channel SNRs. The GFFs in our experiments were carefully designed for the central pump power values (40 mW to 60 mW) to cancel spectral variation in signal and noise power at the end of the longest link. More precise dynamic gain equalization (the wavelength-selective GEF) prevented residual gain differences from accumulating over several spans, ensuring signal stability over the entire link, and similar tunable

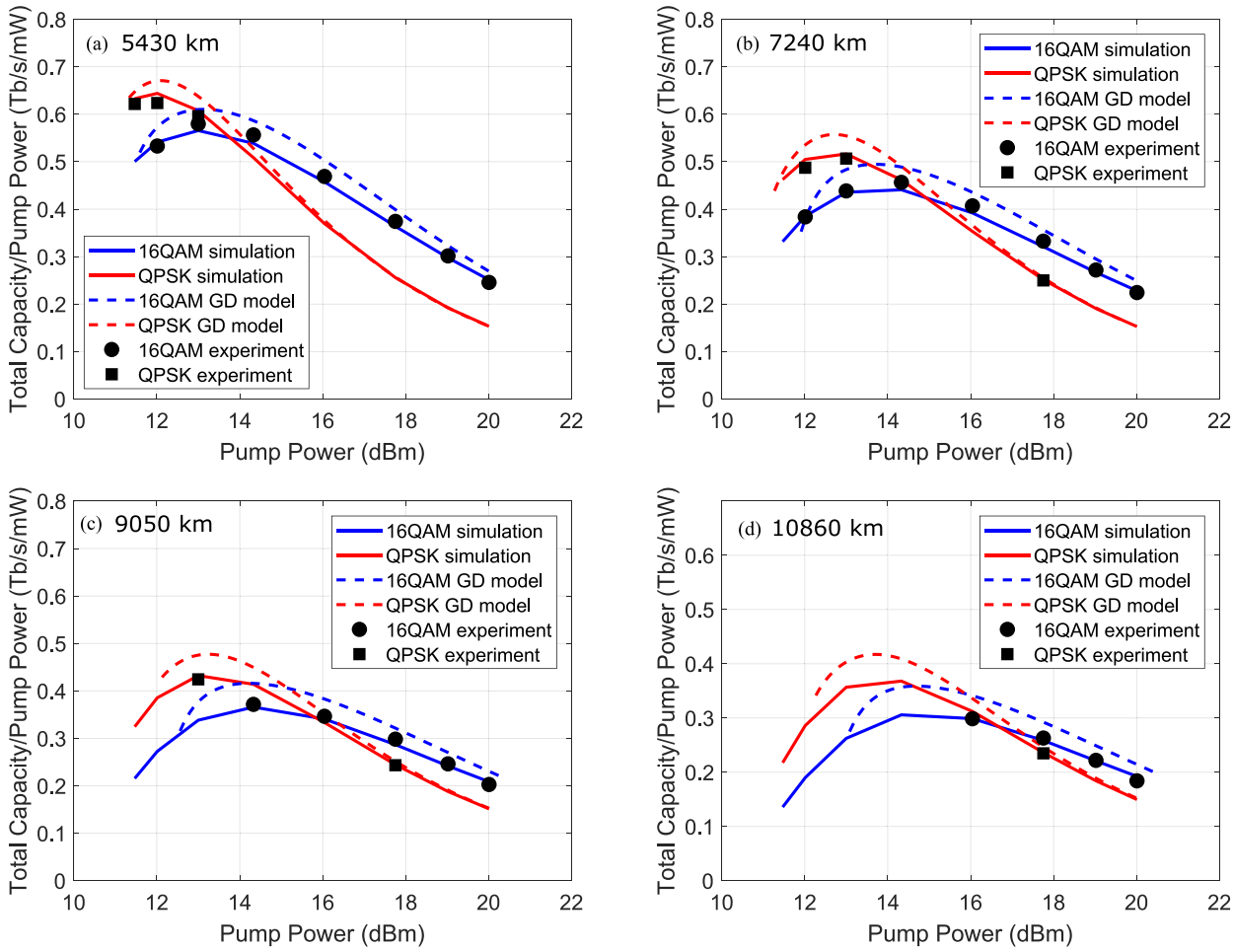

Fig. 9. Experimental system PE metric of capacity per unit pump power C/P_p in Tb/s/mW vs. pump power in dBm, for the link distances a) 5430 km, b) 7240 km, c) 9050 km, and d) 10860 km. Measured experimental data points are shown as black filled circles for 16QAM and squares for QPSK signal formats. Continuous solid curves connect the detailed modeling simulation results, while the simplified model predictions assuming constant-output-power black-box amplifiers with generalized droop (GD model) are shown as the dashed curves, in blue for 16QAM and in red for QPSK signal formats.

approaches have widespread use in currently deployed long-haul links [29]. At lower pump powers, however, the mismatched GFF design and imperfect power balancing in our experiments caused large OSNR variations across the band, which would be improved upon in deployed systems using GFFs specifically designed for the chosen pump power and adaptive compensation of gain tilt and ripple every 10 to 20 spans [29]. An alternative approach avoiding GFFs altogether has been proposed recently in [30] and compared favorably in capacity to that with GFFs for a short-reach system on the order of hundreds of km, but it remains to be seen how this approach would scale for full-band transmission over transoceanic link distances.

B. *Improving PE by Optimization*

Span lengths in long-haul submarine systems typically vary from 40 km to 80 km. While optimizing the span length was outside the scope of our study, which was limited to spans of 60 km, potentially higher power and cost efficiencies could be achieved by optimizing the span length depending on the link length and other design parameters. Therefore, our power efficiency and capacity predictions may be considered lower bounds on the performance achievable if the span lengths were optimized according to link parameters and techno-economic considerations.

We investigated whether further improvement in power efficiency could be gained by optimizing the signal bandwidth and EDF lengths for each pump power and link length using the technique developed in [20], which assumes perfect amplifier gain flattening in each span. As the experimental setup was designed to operate close to optimally within the central range of pump powers using such a technique, allowing for a slight decrease in amplifier length or increase in the signal bandwidth yielded only a minor improvement at higher pump powers. A more significant improvement might be expected when using the ideal GFF profile for each pump power tested, particularly at lower pump powers where the GFF used in the experiments incurred higher wavelength-dependent loss as noted, and when using more homogeneous EDFAs. Simulation assuming the ideal experimental conditions as such, i.e., uniform amplifiers with perfectly matching gain flattening per span and stable, unvarying pump wavelengths, could be used to estimate how much the PE of the links studied might be increased. This was achieved in two steps: a first optimization step in which

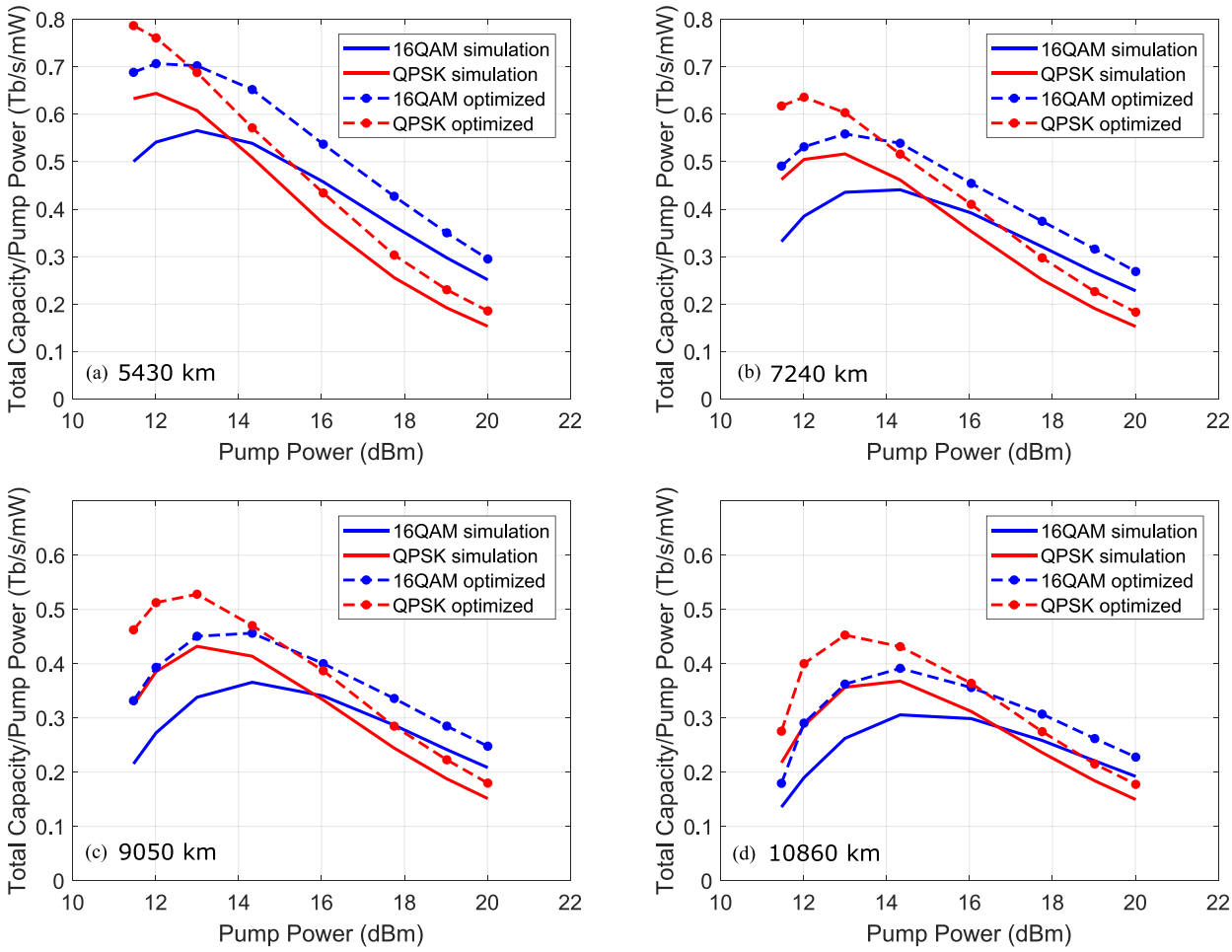

Fig. 10. Simulated experimental system and optimized system PE metric of capacity per unit pump power C/P_p in Tb/s/mW vs. pump power in dBm, for the link distances a) 5430 km, b) 7240 km, c) 9050 km, and d) 10860 km. Continuous blue (16QAM) and red (QPSK) solid curves connect the detailed modeling simulation results as in Fig. 9, while dashed and marked curves of the same color connect the corresponding optimized system predictions.

the EDF length and power allocation were obtained under the above assumptions, followed by a second forward simulation step using these new parameters and assumptions, otherwise keeping the same setup as used to simulate the experiment. The effect of nonlinear noise accumulation was neglected in the first optimization step in order to keep the computation time reasonable and was included in the second evaluation step. The higher noise figure of the two-stage sixth-span amplifier was accounted for in both steps.

In Fig. 10, we show the predicted C/P_p curves under the assumptions of homogeneous amplifiers (with the average excess loss given in Table I) pumped by stable laser diodes and therefore requiring no additional scaling of the amplifier absorption and gain coefficients, with GFF profiles perfectly matching the amplifier gain in each span, and optimally chosen EDF lengths and signal power bandwidths for each pump power and link length. The optimization then yielded, with increasing pump power, an increase in bandwidth from the original 80-channel plan at 11.5 dBm or 14 mW, up to 96 channels (between 1527 nm and 1566 nm) at 20 dBm or 100 mW, with channel powers decreasing from 0.5 dB to 1.2 dB lower than those used in the experiment, and EDFs increasing in length from 5.7 m to 6.2 m.

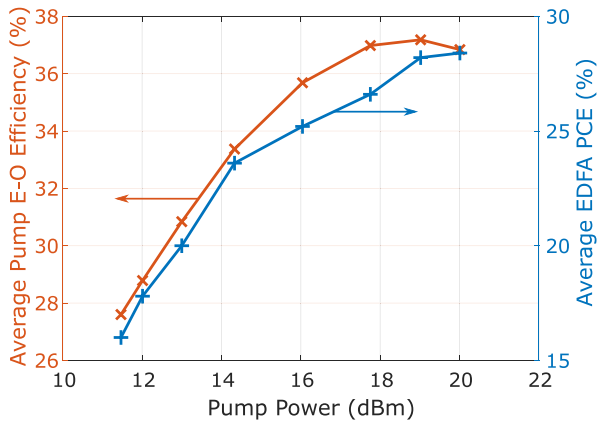

Fig. 11. Dependence on pump power of average measured E-O efficiency of the pump lasers in the recirculating loop (red crosses, left ordinate label), and average measured optical-to-optical EDFA PCE, η_o (blue pluses, right ordinate label).

Implementation penalties from the experimental setup applied to these optimized links as well. The PE results shown are up to 0.2 Tb/s/mW higher than achieved in our experiments at the

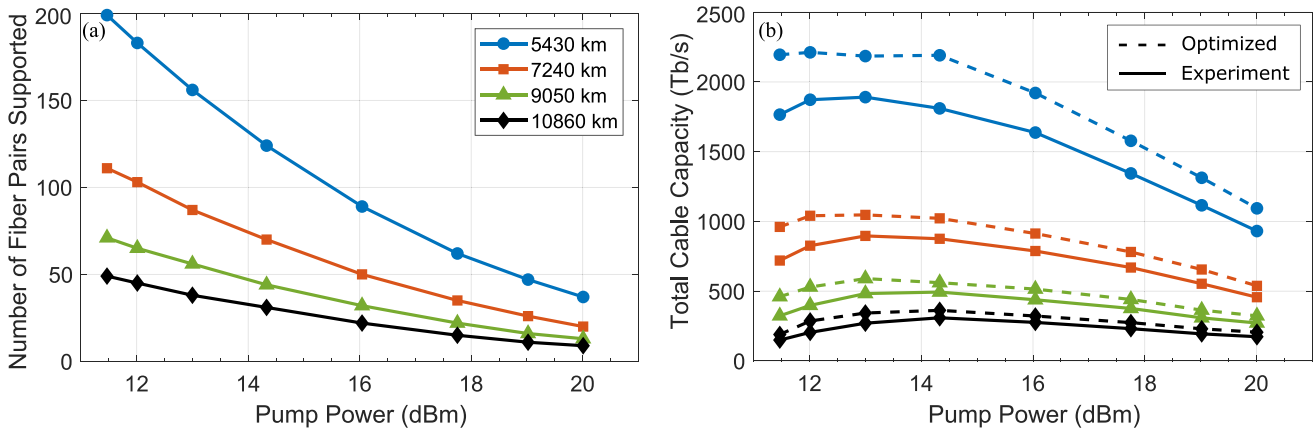

Fig. 12. a) Number of fiber pairs supported F vs. pump power according to expression (4) for the four links of length $L = 5430$ km, 7240 km, 9050 km, and 10860 km. b) Corresponding total cable capacities, taken as the maximum of the 16QAM and QPSK capacities, for the experimental links (solid lines) and optimized links (dashed lines) with the same number of fiber pairs. Calculations assume power-feed voltage $V_{\rm pf} = 15$ kV, cable resistivity $\rho = 1\ \Omega$/km and overhead power fraction per amplifier node $\varepsilon = 10\%$.

lowest pump power, decreasing to around 0.03 Tb/s/mW higher at 20 dBm or 100 mW pump power. We observe optimum PEs between 25% and 30% higher in the case of PM-16QAM, and between 20% and 25% higher in the case of PM-QPSK, at lower optimal pump powers.

C. Projected Cable Capacities

In this section, we provide estimated fiber pair counts and total cable capacities for the four link distances studied according to our experimental results and simulations. We assume typical values for submarine systems of power-feed voltage $V_{\rm pf} = 15$ kV, cable resistivity $\rho = 1\ \Omega$/km for a link length L in km, and overhead power fraction per amplifier node $\varepsilon = 10\%$ [9]. We also assume a loss of 0.3 dB per coupler used in a pump farming approach [26] to reliably pump multiple fiber cores with a bank of lasers, conservatively assumed to be of the same number. From measurements we determined the average electrical-to-optical (E-O) conversion efficiency of the pump lasers to be dependent on pump power as shown by the red curve in Fig. 11. The average slope efficiency of the pump lasers was 0.63 ± 0.07 mW/mA, and the average threshold current was 10 mA, corresponding to an electrical power threshold of 26 mW. The optical-to-optical EDFA PCE is defined as

$$\eta_o = \frac{P_{s,\rm out} - P_{s,\rm in}}{P_p}, \tag{3}$$

where P_p is the pump power, and $P_{s,\rm in}$ and $P_{s,\rm out}$ are the total input and output (here taken after the GFF) signal power over all WDM channels, respectively. The experimentally measured PCE, as shown by the blue curve in Fig. 11, increases with pump power from 16% at 11.5 dBm or 14 mW, to 28% at 20 dBm or 100 mW. Simulated PCE values were within the same range for all five custom amplifiers. For a given link, working backwards from the EDFA+GFF output power, the overall amplifier E-O efficiency η is given by the product of the EDFA PCE η_o, the total coupling loss, the E-O efficiency of the pump laser as above, and its driver current control and supervisory circuitry efficiencies, which are assumed to amount to about 22% [31]. With the values thus summarized, the resulting overall E-O efficiency η increases with pump power from 0.85% at 11.5 dBm to 2% at 20 dBm.

Considering the total electrical power consumed by each amplifier [9], [32], the number of fiber pairs F supported given the above feed-power constraint can be expressed as

$$F = \left\lfloor \frac{(1-\varepsilon)\eta V_{\rm pf}^2}{8N\rho L \eta_o P_p} \right\rfloor, \tag{4}$$

where $\lfloor \cdot \rfloor$ denotes the floor operation, and N is the number of amplifier nodes, one less than the number of spans.

Fig. 12. a) shows the fiber pair count for the four link distances studied, increasing with decreasing pump power. The total cable capacity is then obtained by scaling the capacity per fiber (taken to be the maximum of the 16QAM and QPSK capacities) by the number of fibers supported according to expression (4), and is shown with pump power and distance by the solid curves in Fig. 12. b). For instance, the link of length 9050 km attains a maximum cable capacity of 500 Tb/s when operated at 14.3 dBm or 27 mW pump power with just under 50 fiber pairs. The results of similar calculations for the optimized links according to simulated performance, with virtually the same average EDFA PCEs and therefore fiber counts, are presented as the corresponding dashed curves in Fig. 12. b). For the optimized links of length 7240 km at pump powers near 13 dBm or 20 mW, capacities over 1 Pb/s are achievable using slightly less than 100 fiber pairs, while for the optimized links of length 5430 km at pump powers less than 16 dBm or 40 mW, capacities close to or above 2 Pb/s become feasible.

V. Conclusion

We designed and built a recirculating loop setup and performed extensive experiments to fully explore capacity and power efficiency over a wide range of powers and distances relevant to power-constrained submarine systems. The results showed excellent agreement with detailed modeling including amplifier physics as well as generalized droop, verifying the

existence of an optimal pump power maximizing power efficiency predicted by generalized droop models assuming black-box amplifiers. We also provided best-case estimates of power efficiencies by extending prior long-haul system optimization techniques and assuming ideal operating conditions including perfect gain flattening and uniform EDFAs, showing that power efficiency improvements of about 25% are possible. Finally, by scaling to the number of fibers supported using a power-constrained SDM approach to designing long-haul submarine links, we showed projected transoceanic cable capacities on the order of 1 Pb/s to be feasible at lower pump and amplifier output powers.

ACKNOWLEDGMENT

The authors would like to thank F. A. Barbosa and E. S. Chou for helpful discussions on estimation and computation of GMI, and K. Bennet for helpful discussions on the EDF design.

REFERENCES

[1] S. Grubb, "Submarine cables: Deployment, evolution, and perspectives," in *Proc. Opt. Fiber Commun. Conf.*, 2018, Paper. M1D.1.
[2] A. Pilipetskii, D. Foursa, M. Bolshtyansky, G. Mohs, and N. S. Bergano, "Optical designs for greater power efficiency," in *Proc. SubOptic*, Dubai, 2016, Paper. TH1A.5.
[3] A. Turukhin *et al.*, "105.1 tb/s power-efficient transmission over 14350 km using a 12-core fiber," in *Proc. Opt. Fiber Commun. Conf. Exhib.*, 2016, pp. 1–3.
[4] O. V. Sinkin, A. V. Turukhin, W. W. Patterson, M. A. Bolshtyansky, D. G. Foursa, and A. N. Pilipetskii, "Maximum optical power efficiency in SDM-based optical communication systems," *IEEE Photon. Technol. Lett.*, vol. 29, no. 13, pp. 1075–1077, Jul. 2017.
[5] O. V. Sinkin *et al.*, "SDM for power-efficient undersea transmission," *J. Lightw. Technol.*, vol. 36, no. 2, pp. 361–371, Jan. 2018.
[6] S. Desbruslais, "Maximizing the capacity of ultra-long haul submarine systems," in *Proc. 20th Eur. Conf. Netw. Opt. Commun.*, 2015, pp. 1–6.
[7] E. Mateo, Y. Inada, T. Ogata, S. Mikami, V. Kamalov, and V. Vusirikala, "Capacity limits of submarine cables," in *Proc. SubOptic*, Dubai, 2016, Paper. TH1A.1.
[8] O. D. Domingues, D. A. A. Mello, R. da Silva, S. O. Ari, and J. M. Kahn, "Achievable rates of space-division multiplexed submarine links subject to nonlinearities and power feed constraints," *J. Lightw. Technol.*, vol. 35, no. 18, pp. 4004–4010, Sep. 2017.
[9] J. D. Downie, "Maximum capacities in submarine cables with fixed power constraints for c-band, c l-band, and multicore fiber systems," *J. Lightw. Technol.*, vol. 36, no. 18, pp. 4025–4032, Sep. 2018.
[10] P. J. Winzer, "Energy-efficient optical transport capacity scaling through spatial multiplexing," *IEEE Photon. Technol. Lett.*, vol. 23, no. 13, pp. 851–853, Jul. 2011.
[11] R. Essiambre and R. W. Tkach, "Capacity trends and limits of optical communication networks," *Proc. IEEE Proc. IRE*, vol. 100, no. 5, pp. 1035–1055, May 2012.
[12] R. Dar *et al.*, "Cost-optimized submarine cables using massive spatial parallelism," *J. Lightw. Technol.*, vol. 36, no. 18, pp. 3855–3865, Sep. 2018.
[13] M. A. Bolshtyansky *et al.*, "Single-mode fiber SDM submarine systems," *J. Lightw. Technol.*, vol. 38, no. 6, pp. 1296–1304, Mar. 2020.
[14] H. Zhang *et al.*, "Power-efficient 100 gb/s transmission over transoceanic system," *J. Lightw. Technol.*, vol. 34, no. 8, pp. 1859–1863, Apr. 2016.
[15] A. Turukhin *et al.*, "Demonstration of potential 130.8 tb/s capacity in power-efficient SDM transmission over 12700 km using hybrid micro-assembly based amplifier platform," in *Proc. Opt. Fiber Commun. Conf.* Opt. Soc. Amer., 2019, Paper. M2I.4.
[16] A. Pilipetskii, M. Bolshtyansky, D. Foursa, and O. Sinkin, "SDM power-efficient ultra high-capacity submarine long haul transmission systems (tutorial)," in *Proc. Opt. Fiber Commun. Conf.* Opt. Soc. Amer., 2020, Paper. M3G.5.
[17] J.-C. Antona, A. C. Meseguer, and V. Letellier, "Transmission systems with constant output power amplifiers at low SNR values: A generalized droop model," in *Proc. Opt. Fiber Commun. Conf.* Opt. Soc. Amer., 2019, Paper. M1J.6.
[18] A. Bononi, J.-C. Antona, M. Lonardi, A. Carbo-Meseguer, and P. Serena, "The generalized droop formula for low signal to noise ratio optical links," *J. Lightw. Technol.*, vol. 38, no. 8, pp. 2201–2213, Apr. 2020.
[19] J. D. Downie, X. Liang, V. Ivanov, P. Sterlingov, and N. Kaliteevskiy, "SNR model for generalized droop with constant output power amplifier systems and experimental measurements," *J. Lightw. Technol.*, vol. 38, no. 12, pp. 3214–3220, Jun. 2020.
[20] J. K. Perin, J. M. Kahn, J. D. Downie, J. Hurley, and K. Bennett, "Importance of amplifier physics in maximizing the capacity of submarine links," *J. Lightw. Technol.*, vol. 37, no. 9, pp. 2076–2085, May 2019.
[21] A. Alvarado, T. Fehenberger, B. Chen, and F. M. J. Willems, "Achievable information rates for fiber optics: Applications and computations," *J. Lightw. Technol.*, vol. 36, no. 2, pp. 424–439, Jan. 2018.
[22] J. D. Downie *et al.*, "Experimental characterization of power efficiency for power-limited SDM submarine transmission systems," in *Proc. 46th Eur. Conf. Opt. Commun.*, 2020, Paper. Tu2E.5.
[23] C. R. Giles and E. Desurvire, "Modeling erbium-doped fiber amplifiers," *J. Lightw. Technol.*, vol. 9, no. 2, pp. 271–283, Feb. 1991.
[24] E. Desurvire, Erbium-Doped Fiber Amplifiers: Principles and Applications. Hoboken, NJ, USA: Wiley, 1994.
[25] E. Desurvire, D. Bayart, B. Desthieux, and S. Bigo, Erbium-Doped Fiber Amplifiers: Device and System Developments. Hoboken, NJ, USA: Wiley, 2002.
[26] P. Pecci *et al.*, "Pump farming as enabling factor to increase subsea cable capacity," in *Proc. SubOptic*, 2019, Paper OP14-4.
[27] N. S. Bergano, B. Dean, L. Garrett, M. E. Kordahi, H. Li, and B. Nyman, "Submerged plant equipment," in *Undersea Fiber Communications Systems*, J. Chesnoy, Ed. Elsevier, 2016, ch. 12.
[28] S. Mohrdiek *et al.*, "Reliability culture of cost effective 980 nm submarine pumps," in *Proc. SubOptic*, 2007, Paper WE3.13.
[29] D. Bayart, "Opt. amplification," in *Undersea Fiber Communications Systems*, J. Chesnoy, Ed. Elsevier, 2016, ch. 4.
[30] J. Cho *et al.*, "Supply-power-constrained cable capacity maximization using multi-layer neural networks," *J. Lightw. Technol.*, vol. 38, no. 14, pp. 3652–3662, Jul. 2020.
[31] T. Frisch and S. Desbruslais, "Electrical power, a potential limit to cable capacity," in *Proc. SubOptic*, 2013, Paper Tu1C04.
[32] J. D. Downie, X. Liang, and S. Makovejs, "Examining the case for multicore fibers in submarine cable systems based on fiber count limits," *IEEE J. Sel. Top. Quantum Electron.*, vol. 26, no. 4, pp. 1–9, Jul./Aug. 2020.

Hrishikesh Srinivas (Student Member, IEEE) received the B.E. degree in photonic engineering and the B.Sc. degree in mathematics and physical science from the University of New South Wales, Sydney, NSW, Australia, in 2017, and the M.S. degree in electrical engineering from Stanford University, Stanford, CA, USA, in 2019, where he is currently working toward the Ph.D. degree. His current research interests include optical fiber communications, optical amplifier physics, and photonics.

John D. Downie (Member, IEEE) received the B.S. degree in optics from the University of Rochester, Rochester, NY, USA, in 1983, the Certificate of Postgraduate Study in physics from Cambridge University, Cambridge, U.K., in 1984, and the M.S. and Ph.D. degrees in electrical engineering from Stanford University, Stanford, CA, USA, in 1985 and 1989, respectively. In 1989, he joined the National Aeronautics and Space Administration Ames Research Center, where he was a Research Scientist and the Group Leader of the Information Physics Research Group. He joined Corning Incorporated in 1999 and is a Principal Scientist with the Science and Technology Division. He has authored and coauthored around 190 journal and conference papers to date. His current research interests with Corning Inc. include optical fibers and transmission systems for all length scales. Dr. Downie has been a member of the Optical Society of America since 1984, and currently a Senior Member since 2007. He is a Reviewer for the IEEE and OSA optics journals.

Jason E. Hurley received the Associates of Applied Science degree in electronics technology from the Pennsylvania College of Technology, Williamsport, PA, USA, in 1996 and the B.Sc. degree in electrical engineering from Alfred University, Alfred, NY, USA, in 2008. In 1997, he joined the Science and Technology Division, Corning Inc. He is currently a Senior Scientist with the Optical & Wireless Transmission Group, focusing on fiber characteristics to improve system performance on single mode and multimode fibers. He has coauthored more than 50 journals and conference articles, and has eight patents in the field of optical communications.

Xiaojun Liang received the B.Sc. degree in optoelectronics and the M.A.Sc. degree in optical engineering from the Huazhong University of Science and Technology, Wuhan, China, in 2008 and 2010, respectively, and the Ph.D. degree in electrical and computer engineering from McMaster University, Hamilton, ON, Canada, in 2015. In 2015, he joined Corning Incorporated and is currently a Senior Optical Scientist with the Science and Technology Division, Corning, NY, USA. He has coauthored more than 40 journal and conference papers. His current research interests include high data rate optical transmission systems and digital signal processing techniques.

James Himmelreich, biography not available at the time of publication.

Jose Krause Perin biography not available at the time of publication.

Darli A. A. Mello (Member, IEEE) graduated in electrical engineering from the University of Campinas (Unicamp), Campinas, Brazil, in 2000. He received the M.Sc. degree from the Munich University of Technology, Munich, Germany, in 2002, and the Ph.D. degree from Unicamp. During his master's degree, he carried out both experimental and theoretical work with the Siemens Research Labs, Munich, Germany. After his Ph.D. studies, he spent one year with Padtec S/A as a Senior Technology Engineer. From August 2008 to March 2014, he was an Assistant Professor with the University of Brasilia, Brasilia, Brazil. He is currently an Assistant Professor with the School of Electrical and Computer Engineering, Unicamp. In 2019, he was a Visiting Scholar with Stanford University, Stanford, CA, USA, where he worked on coupled SDM transmission. His research interests include optical transmission and networking. He was a Technical Program Committee (TPC) Member of several conferences, including OFC, ACP, ICC, and Globecom. He was the TPC Co-Chair of SBrT 2011, Imoc 2017, and the Optical Communications Subcommittee of LAOP 2016 and 2018.

Joseph M. Kahn (Fellow, IEEE) received the A.B., M.A., and Ph.D. degrees in physics from the University of California, Berkeley, CA, USA, in 1981, 1983, and 1986, respectively. From 1987 to 1990, he was with AT&T Bell Laboratories. In 1989, he demonstrated the first successful synchronous (i.e., coherent) detection using semiconductor lasers, achieving record receiver sensitivity. From 1990 to 2003, he was with Electrical Engineering and Computer Sciences Faculty, Berkeley. In 1992, he demonstrated the coherent detection of QPSK. In 1999, D.-S. Shiu and Kahn authored or coauthored the first work on probabilistic shaping for optical communications. In 1990 and early 2000, Kahn and collaborators performed seminal work on indoor and outdoor free-space optical communications and multiinput multioutput wireless communications. In 2000, Kahn and K.-P. Ho founded StrataLight Communications, whose 40 Gb/s-per-wavelength long-haul fiber transmission systems were deployed widely by AT&T, Deutsche Telekom, and other carriers. In 2002, Ho and Kahn applied to patent the first electronic compensation of fiber Kerr nonlinearity. StrataLight was acquired by Opnext in 2009. In 2003, Kahn became a Professor of electrical engineering with the E. L. Ginzton Laboratory, Stanford University, Stanford, CA, USA. He and collaborators have extensively studied rate-adaptive coding and modulation, as well as digital signal processing for mitigating linear and nonlinear impairments in coherent systems. In 2008, E. Ip and Kahn (and G. Li independently) invented simplified digital backpropagation for compensating fiber Kerr nonlinearity and dispersion. Since 2004, Kahn and collaborators have been studying propagation, modal statistics, spatial multiplexing and imaging in multimode fibers, elucidating principal modes, and demonstrating transmission beyond the traditional bandwidth-distance limit in 2005, deriving the statistics of coupled modal group delays and gains in 2011, and deriving resolution limits for imaging in 2013. His current research interests include optical frequency comb generators, coherent data center links, rate-adaptive access networks, fiber Kerr nonlinearity mitigation, ultra-long-haul submarine links, and optimal free-space transmission through atmospheric turbulence. He was the recipient of the National Science Foundation Presidential Young Investigator Award in 1991.